Journal of Power Sources 243 (2013) 274–279

Contents lists available at SciVerse ScienceDirect

Journal of Power Sources

journal homepage: www.elsevier.com/locate/jpowsour

Synthesis, morphological analysis and electrochemical performance of iron hydroxyl phosphate as a cathode material for lithium ion batteries

Shi Ming Zhang, Jun Xi Zhang*, Suo Jiong Xu, Xu Jie Yuan, Tian Tan

Electrochemical Research Group, Shanghai University of Electric Power, Shanghai 200090, China

HIGHLIGHTS

- A new iron hydroxyl phosphate cathode material was synthesized by a sample hydrothermal method.
- We obtained the spherical, cubic, multi-armed and cross-like morphology by adjusting the hydrothermal temperatures.
- Iron hydroxyl phosphate exhibited a reversible initial discharge specific capacities of 176 mAh g^{-1}.
- The specific capacity retained about 95% of the initial discharge specific capacity after 60 cycles at 0.1C.
- The spherical morphology and smaller particle size can improve the electrochemical performances.

ARTICLE INFO

Article history:
Received 6 March 2013
Received in revised form
13 May 2013
Accepted 30 May 2013
Available online 13 June 2013

Keywords:
Iron hydroxyl phosphate
Morphology control
Hydrothermal temperature
Cathode material

ABSTRACT

Iron hydroxyl phosphate, with the formula $Fe_{1.5}(PO_4)(OH)$, used as a cathode material in lithium ion batteries, is synthesised by a sample hydrothermal method. Scanning electron microscopy (SEM), X-ray diffraction and galvanostatical charge/discharge tests are employed to characterise the morphology, structure and electrochemical performance of the iron hydroxyl phosphate, respectively. FE-SEM shows that the morphologies are closely related to the hydrothermal temperatures at which they are synthesised. The morphologies, such as spherical, cubic, multi-armed and cross-like structures, could be easily regulated by adjusting the hydrothermal temperature. It is found that different morphologies of iron hydroxyl phosphate gave rise to different electrochemical performances. Compared to the others, iron hydroxyl phosphate spherical composites exhibit not only a high reversible capacity but also good cycling stability, with a reversible initial discharge specific capacity of around 176 mAh g^{-1} and a remaining 95% of the initial discharge specific capacity after 60 cycles at 0.1C. The improved electrochemical performance is attributed to the spherical morphology and smaller particle size, which increase the reaction interfaces and shorten the diffusion distance of the lithium ions.

1. Introduction

The use of lithium ion batteries for stationary energy storage systems to complement renewable energy sources such as solar and wind power has recently attracted great interest. These batteries are perceived as an efficient energy storage device as it has the ability to store and release electric energy with high density and reversibility [1].

$LiFePO_4$, a cathode material for lithium ion battery, has a theoretical capacity of 170 mAh g^{-1}, combined with a lithium intercalation potential of 3.5 V [2]. Since the pioneering works of Padhi et al. [2], great effort has been devoted to the olivine type of $LiFePO_4$, with three-dimensional poly-anion frameworks built from octahedral FeO_6 and tetrahedral PO_4. For $LiFePO_4$, the extraction/insertion mechanism can be described as the two-phase behaviour of the $LiFePO_4$—$FePO_4$ system. $LiFePO_4$ can de-intercalate 1 M Li^+ ions per formula unit, corresponding to the phase transformation from $LiFePO_4$ to $FePO_4$, which maintains nearly the same structure: *a* and *b* lattice constants decrease slightly while *c* increases [3]. Therefore, $FePO_4$ has been proposed to be a suitable cathode material for lithium batteries [4]. Some studies on $FePO_4$ cathode materials indicate that amorphous $FePO_4$ has a high electrochemical activity [5,6]. However, amorphous $FePO_4$ also suffers from varying levels of capacity due to its amorphous structure [7].

Like $FePO_4$, iron hydroxyl phosphate can be used as cathode material for lithium ion batteries [8]. There are lots of advantages for its use in lithium ion batteries. Firstly, iron hydroxyl phosphate has a higher theoretical specific capacity than $FePO_4$ and $LiFePO_4$. Secondly, it is a binary system and Fe (III) compounds are raw

* Corresponding author. Tel./fax: +86 21 65700719.
E-mail address: zhangjunxi@shiep.edu.cn (J.X. Zhang).

0378-7753/$ – see front matter © 2013 Elsevier B.V. All rights reserved.
http://dx.doi.org/10.1016/j.jpowsour.2013.05.154

materials, the sources of which are easily available. In addition, its synthesis is simple, without any need for a protective atmosphere, saving on both equipment and overall costs [9].

Iron hydroxyl phosphates are well known minerals. The natural minerals include barbosalite $Fe_3(PO_4)_2(OH)_2$ [10,11], rockbridgeite $Fe_5(PO_4)_3(OH)_5$ [12], beraunite $Fe_6(PO_4)_4(OH)_5{\cdot}6H_2O$ [13,14] and whitmoreite $Fe_3(PO_4)_2(OH)_2{\cdot}4H_2O$ [15]. The structure of some of the minerals is not fully known, such as that of giniite $Fe_5(PO_4)_4(OH)_2{\cdot}2H_2O$. Some of them have various compositions with the same structure, such as the synthetic ferric giniite with its composition ranging from $Fe_{4.52}(PO_4)_4(OH)_{1.56}(H_2O)_{2.75}$ to $Fe_5(PO_4)_4(OH)_3(H_2O)_{4.6}$ [16].

Recently, iron hydroxyl phosphate has been proposed as cathode material for lithium ion batteries. Dolle et al. [17] reported that $Fe_{1.19}PO_4F_{0.11}(OH)_{0.46}(H_2O)_{0.43}$ was a candidate cathode material for lithium ion battery with a theoretical specific capacity of 180 mAh g^{-1} and an average potential plateau of 2.8 V vs. Li^+/Li. Song et al. [15] revealed that iron (III) hydroxyl phosphate, of the general formula $Fe_{2y-y}(PO_4)\ (OH)_{3-3y}(H_2O)_{3y-2}$ ($y = 2/3$ or 0.82, □ represents vacancy), showed reversible capacities of 150 mAh g^{-1}($y = 2/3$) and 100 mAh g^{-1} ($y = 0.82$), respectively. Wang et al. [8] discovered that $Fe_5(PO_4)_4(OH)_3{\cdot}2H_2O$ had higher electronic conductivity than $LiFePO_4$ using GGA + U calculations. All these reports showed that iron hydroxyl phosphate used as iron-based cathode material for lithium ion batteries held huge promise. In this work, we explored the synthesis, morphological regulation and electrochemical properties of the iron hydroxyl phosphate $Fe_{1.5}(PO_4)(OH)$, which has not been used before as cathode material. We demonstrated a relationship between morphology and hydrothermal temperature. We also reported the influence of morphology and size on the electrochemical properties of iron hydroxyl phosphate.

2. Experimental

The iron hydroxyl phosphate samples were synthesised by a hydrothermal route. Here, 0.01 mol L^{-1} $Fe(NO_3)_3{\cdot}9H_2O$ (AR) solution, 0.01 mol L^{-1} $NH_4H_2PO_4$ (AR) and 0.001 g sodium dodecyl benzene sulphonate (SDBS) were added to 100 mL of distilled water under constant stirring at 350 r/min for 10 min at room temperature. The initial pH values of the solutions were adjusted to 2.5 by adding $NH_3{\cdot}H_2O$ (1:1). The reaction mixtures were then sealed into a 125 ml Teflon-lined stainless steel autoclave and heated at 150 °C–170 °C–180 °C and 200 °C for 24 h and then cooled slowly to room temperature. The powders were obtained by centrifugal separation and washed with ethanol three times to remove the solvent. The precipitates were dried at 100 °C for 12 h and then sintered under an air atmosphere at 400 °C for 3 h.

The crystal phases were identified using X-ray diffraction (D8 Advance, Bruker Germany) by Cu Kα radiation with 2θ ranging from 20° to 90° at a scan rate of 2°/min at room temperature. The surface morphology of the particles was characterised using field emission-scanning electron microscopy (SEM) (SU70, Japan). The determination of the electrochemical properties of the synthesised iron hydroxyl phosphates was accomplished by assembling CR2016 coin cells. The composite positive electrodes were prepared by ball-milling a mixture of the active materials, conductive material (acetylene black) and binder (polytetra-fluoroethylene, PTFE) at a weight ratio of 75:17:8. The average mass of composite loading on to the electrode was 15 mg; the electrode sheet was then dried in a vacuum oven at 120 °C for 24 h. Finally, coin-type cells were assembled in a glove box (RH < 0.1%, at 20 °C), which used lithium foil as the anode, Celgard 2400 microporous polypropylene film as the separator, and 1 M $LiPF_6$ in PC/DEM (1:1) as the electrolyte. Charge-discharge tests were performed between 2.0 V and 4.0 V using the Land Battery test system (Wuhan LAND, China). The AC perturbation signal was 5 mV and the frequency range was from 0.01 Hz to 100 kHz. All the tests were performed at room temperature (25 °C).

3. Results and discussion

Fig. 1a displays the XRD patterns of $Fe_{1.5}(PO_4)(OH)$ samples prepared at different hydrothermal temperatures. The well-defined series of peaks indicate a tetrahedral crystalline $Fe_{1.5}(PO_4)(OH)$ structure with lattice parameters of $a = 5.28$ Å and $c = 12.83$ Å, which is consistent with the values in the literature [11]. The peak on the (0 0 4) crystal face increasingly strengthens with an increase in the hydrothermal temperature, and is at its strongest at 180 °C and then decreases again at 200 °C, which may be attributed to the crystal growth on the (0 0 4) crystal face and the increase in crystallinity, as

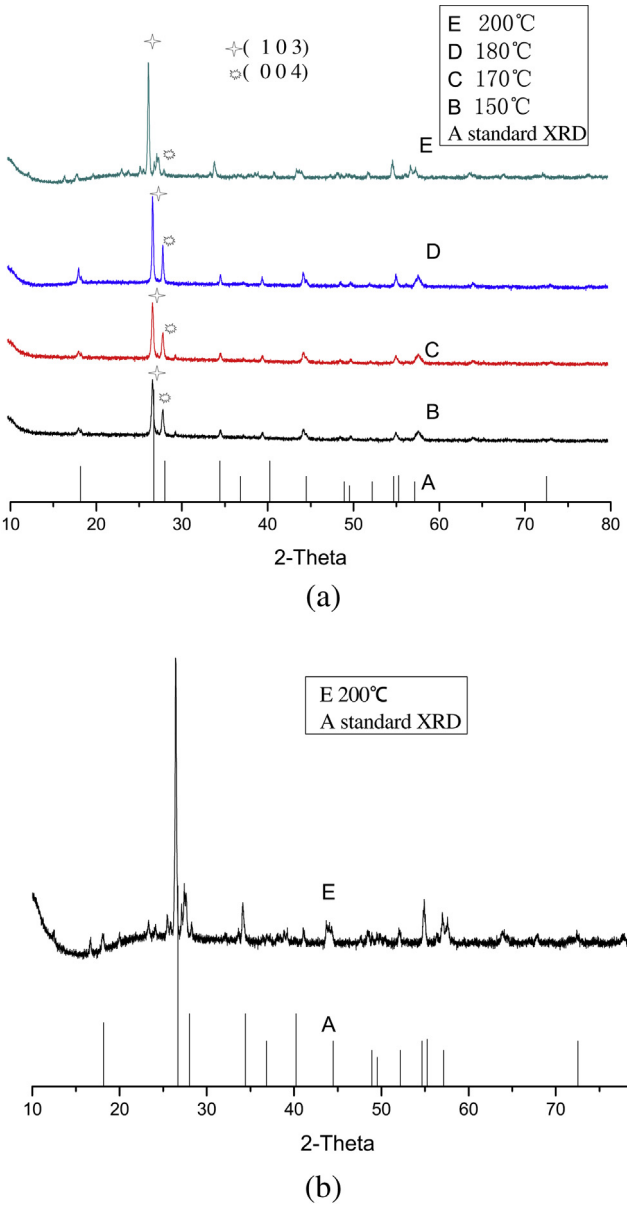

Fig. 1. (a) The XRD patterns of $Fe_{1.5}$ (PO_4) (OH) samples prepared at different hydrothermal temperatures; (b) the XRD patterns of $Fe_{1.5}(PO_4)(OH)$ samples prepared with hydrothermal at 200 °C.

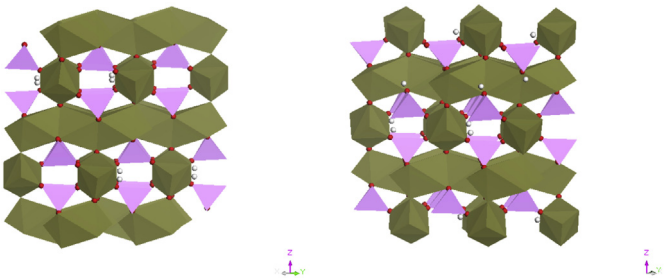

Fig. 2. Polyhedral views of $Fe_{1.5}(PO_4)(OH)$ along the directions [1 1 0] and [−1 1 0].

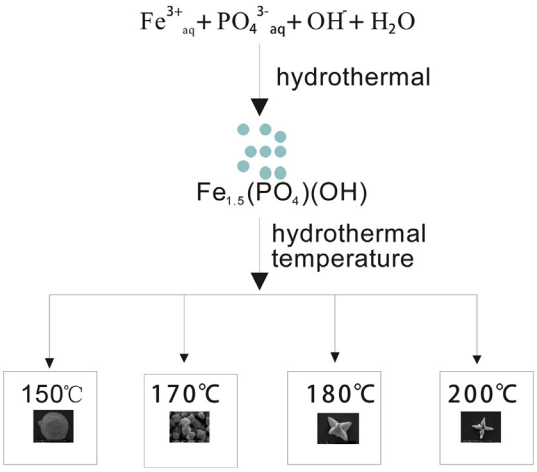

Fig. 3. Summary of results obtained in the iron hydroxyl phosphate system as a function of hydrothermal temperature. The morphology of the synthesized solid is indicated by the schematic illustration in each box.

well as the peak on the (1 0 3) crystal face increasingly strengthening with a rising hydrothermal temperature.

Fig. 1b shows the XRD patterns of $Fe_{1.5}(PO_4)(OH)$ samples prepared at a hydrothermal temperature of 200 °C. There are some other phases in the sample under this hydrothermal condition, which may be due to the transformation of $Fe_{1.5}(PO_4)(OH)$ at this temperature.

Polyhedral views of $Fe_{1.5}(PO_4)(OH)$ are shown in Fig. 2. The structure is formed by octahedral FeO_6 sharing opposite faces in infinite chains along the directions [1 1 0] and [−1 1 0], respectively. The chains are connected to other chains by overlapping corners between octahedral FeO_6 and tetrahedral FeO_4. These structural features could enhance the compound's electronic conductivity relative to that of the highly insulating olivine, $LiFePO_4$, in which only FeO_6 units share corners [17].

The effects of hydrothermal temperature on the morphology and particle size of the resulting products were investigated. To assess the formation processes of $Fe_{1.5}(PO_4)(OH)$, different hydrothermal temperatures were used.

The precipitation reactions under hydrothermal conditions for $Fe_{1.5}(PO_4)(OH)$ are given by Fig. 3. From the reaction processes, we can see that the hydrothermal temperature played an important role in the growth and morphology of the crystal. It is well known that the solubility of $Fe_{1.5}(PO_4)(OH)$ changes with the temperature and pressure. Thus, changing the hydrothermal temperature also affect the temperature and pressure of the system. Crystallisation involves nucleation and crystal growth. However, the nucleation is related to the super saturation of the reaction solution. Moreover, the activation energy of each crystal surface is also affected by the hydrothermal temperature. Hence, differences in the reaction units of the system due to variations in the hydrothermal temperature give rise to the formation of different morphologies and sizes of $Fe_{1.5}(PO_4)(OH)$.

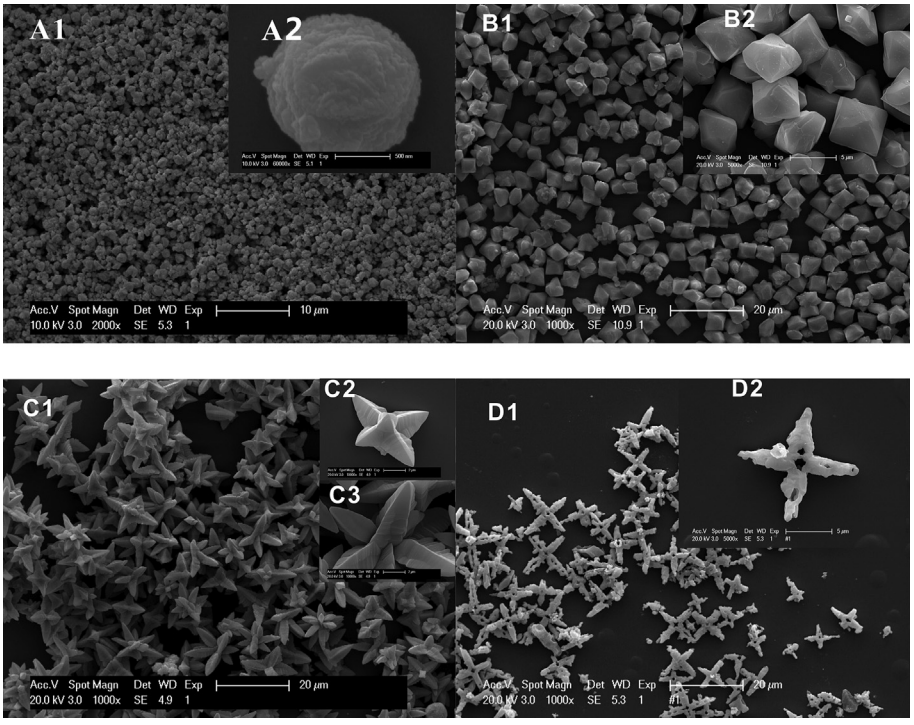

Fig. 4. SEM images of the resulting products synthesized with hydrothermal at different temperatures (A) 150 °C, (B)170 °C, (C)180 °C, (D)200 °C.

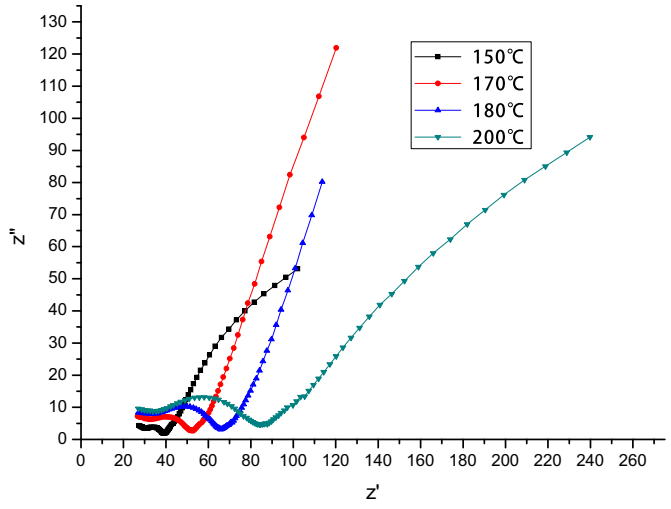

Fig. 5. Nyquist plots for the samples synthesized at different hydrothermal temperatures in the range of 0.01 HZ to 10^5 HZ.

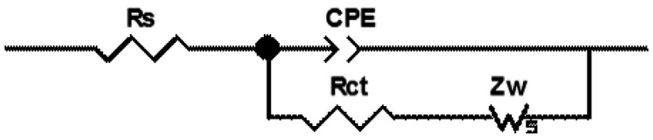

Fig. 6. Equivalent circuit used for simulating the experimental impedance date.

According to the FE-SEM images, shown in Fig. 4, the morphologies and sizes of $Fe_{1.5}(PO_4)(OH)$ varied with the hydrothermal temperature of the reaction solutions.

The morphology of the sample synthesised at 150 °C is shown in Fig. 4A, where very uniform spherical particles can be seen. A high-magnification SEM image in the inset of Fig. 4A, A2, shows that the average particle size was around 1 μm. The surfaces of the particles were coarse, which may have been due to the aggregation of several nano-sized primary $Fe_{1.5}(PO_4)(OH)$ particles forming large secondary particles.

When the hydrothermal temperature of the reaction solution increased to 170 °C, as shown in Fig. 4B, the morphology was cubic with uniform distribution and a diameter of 4 μm.

However, at 180 °C, six-armed structures coexisting with other multi-armed structures (Fig. 4C) and with a size of around 10 μm were formed. Interestingly, four-armed symmetrical structures were clearly observed under high-magnification SEM (the inset in Fig. 4C, shown in Fig. 4C2, C3). No branches were found on the surface of the arms. The multi-armed structure may have been due to crystal growth on the (0 0 4) and (1 0 3) crystal faces, as shown in Fig. 1.

Fig. 4D gives the SEM image of the product synthesised at 200 °C. Lots of cross-like structures were noted in the resulting product. Each cross was composed of four branches and with a hole in the middle. A high-magnification SEM image in the inset of Fig. 4D (as shown in Fig. 4D1) reveals that the surfaces of the branches were irregular, the branches having a diameter of 2 μm and a length of 5 μm, and the highest size of the structure ranging to 12 μm. This

Table 1
Evaluated impedance parameters according to the equivalent circuit of Fig. 6.

Sample $Fe_{1.5}(PO_4)(OH)$	150 °C	170 °C	180 °C	200 °C
R_s (Ω)	27.19	28.82	27.31	28.34
CPE-T	0.00022543	0.00078226	0.00075667	0.00046372
CPE-P	0.68748	0.40398	0.67267	0.39194
R_{ct} (Ω)	14.21	25.24	37.53	75.67

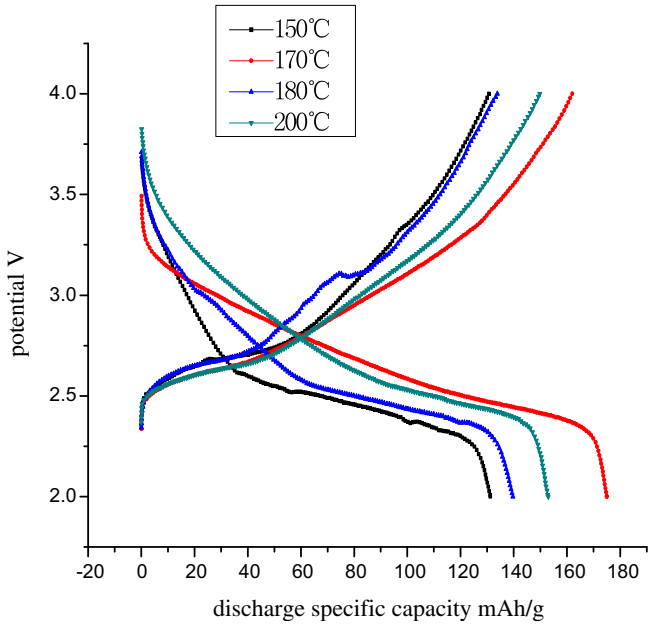

Fig. 7. The initial charge and discharge of $Fe_{1.5}(PO_4)(OH)$ cathode materials prepared at different hydrothermal temperatures at 0.1C.

transformation from a multi-armed structure to a cross one could have been due reduced crystal growth on the (0 0 4) crystal face, while the increase in the tall size of the structure may have been due to further crystal growth on the (1 0 3) crystal face.

Fig. 5 presents the Nyquist plots of $Fe_{1.5}(PO_4)(OH)$ cathode materials generated at different pH values. The Nyquist plots displayed a small intercept at high frequencies, a partial semicircle at high and medium frequencies, and a linear pattern at low frequencies.

The equivalent circuit used in this work is given in Fig. 6, where R_S represents the electrolyte resistance, CPE and R_{ct} represents the double layer capacitance and charge transfer resistance, respectively, and Z_W represents the diffusion-controlled Warburg impedance [18]. The evaluated impedance parameters according to the equivalent circuit in Fig. 6 are presented in Table 1. It can be seen from Table 1 that the R_{ct} values of $Fe_{1.5}(PO_4)(OH)$ samples produced at different hydrothermal temperatures 150 °C, 170 °C, 180 °C and 200 °C were 14.21 Ω, 25.24 Ω, 37.53 Ω and 75.67 Ω,

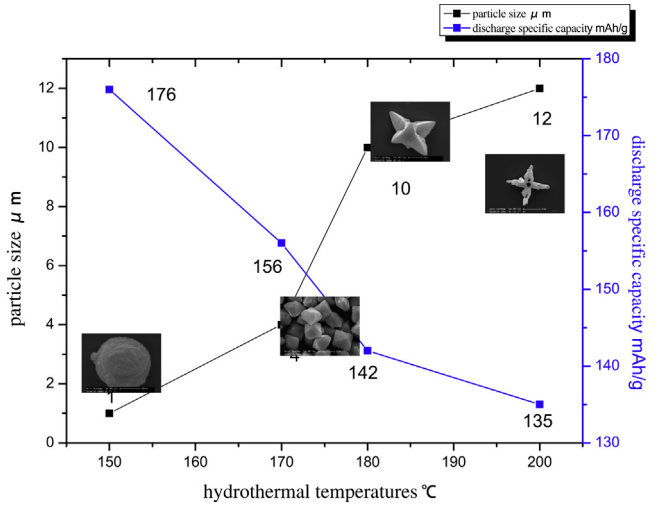

Fig. 8. The relationships between morphology, particle size and discharge specific capacity.

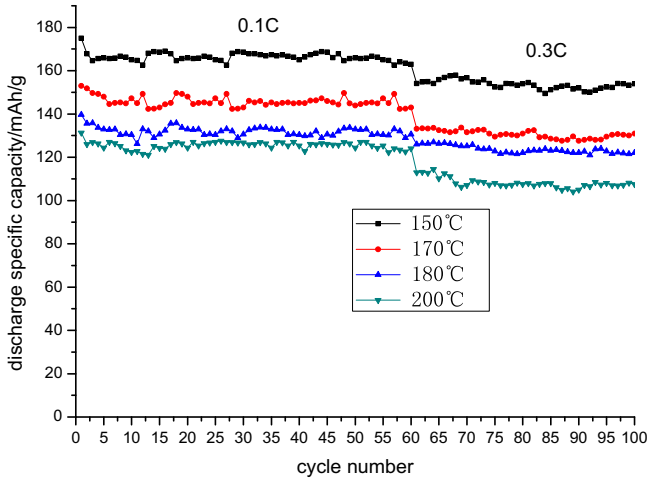

Fig. 9. Discharge capacities versus cycle number curves of $Fe_{1.5}$ (PO_4) (OH) cathode materials prepared at different hydrothermal temperatures at 0.1C and 0.3C.

respectively. The R_{ct} values increased with an increase in the hydrothermal temperature. The R_{ct} value of the sample made at 200 °C was nearly 4 times than that of the compound synthesised at 150 °C. The reasons may be due to the larger specific surface area of the small grain size, which increases the reaction interface to enhance the electrochemical activity of the $Fe_{1.5}(PO_4)(OH)$ electrode. These results reveal that grain size and morphology greatly influenced the electron conductivity of $Fe_{1.5}(PO_4)(OH)$ cathode materials.

Fig. 7 shows the charge/discharge curves of $Fe_{1.5}(PO_4)(OH)$ cathode materials prepared at different hydrothermal temperatures of 150 °C, 170 °C, 180 °C and 200 °C in the range of 2.0–4.2 V at 0.1C. As Fig. 7 shows, the discharge specific capacities of $Fe_{1.5}(PO_4)(OH)$ cathode materials prepared at 150 °C, 170 °C, 180 °C and 200 °C were around 176 mAh g^{-1}, 156 mAh g^{-1}, 142 mAh g^{-1} and 135 mAh g^{-1}, respectively. The results indicate that the specific capacity of $Fe_{1.5}(PO_4)(OH)$ cathode materials decreased with the hydrothermal temperature. The sample prepared at 150 °C showed the highest discharge capacity of 176 mAh g^{-1} for the first cycle at 0.1C.

Fig. 8 shows the relationships between morphology, particle size and discharge specific capacity.

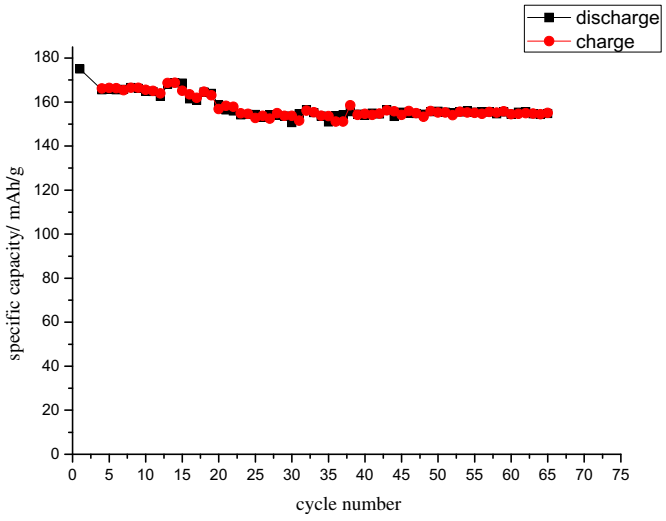

Fig. 10. The charge/discharge specific capacity vs the number of cycle.

These demonstrate that small grain size and spherical morphology can effectively enhance the electrochemical properties of $Fe_{1.5}(PO_4)(OH)$ cathode materials.

From the charge and discharge curves, we also found that the initial charge capacities were higher than the discharge capacities because the $Fe_{1.5}(PO_4)(OH)$ cathode materials must discharge first, corresponding to the lithium ion transferring from the anode material to the $Fe_{1.5}(PO_4)(OH)$ cathode material to format the lithium-containing compounds, and then charge. During the initial discharge process, there are some other side reactions occurring resulting in the loss of capacities during the later charge process.

The discharge capacity versus cycle number curves in the range of 2.0–4.2 V at 0.1C and 0.3C display that the $Fe_{1.5}(PO_4)(OH)$ cathode materials prepared at different hydrothermal temperatures of 150 °C, 170 °C, 180 °C and 200 °C demonstrated good cyclic stability (Fig. 9). The initial discharge capacity of the sample prepared at 150 °C was 176 mAh g^{-1} and the remaining capacity of 165 mAh g^{-1} was nearly 95% of the initial discharge specific capacity after 60 cycles at 0.1C. At 0.3C, the initial discharge capacity of the sample prepared at 150 °C was 159 mAh g^{-1}, with the remaining capacity of 150 mAh g^{-1} being nearly 94% of the initial discharge specific capacity after 40 cycles. At the same discharge rate, the samples prepared at 170 °C–180 °C and 200 °C also exhibited excellent reversibility and cyclic stability. The reasons may be due to the larger specific surface area of the small grain size, which increases the reaction interfaces to enhance the electrochemical activity of the $Fe_{1.5}(PO_4)(OH)$ electrode.

The Fig. 10 shows the charge/discharge specific capacity vs the number of cycle. Which also proved the columbic efficiency of $Fe_{1.5}(PO_4)(OH)$ electrode during the charge/discharge process. From the curves, we obtained that the columbic efficiency of $Fe_{1.5}(PO_4)(OH)$ electrode was near 100%. The result also investigated the excellent reversibility and cyclic stability of $Fe_{1.5}(PO_4)(OH)$ electrode.

4. Conclusion

Iron hydroxyl phosphate with a formula of $Fe_{1.5}(PO_4)(OH)$ was synthesized by a sample hydrothermal method, and the various morphologies were by adjusting the hydrothermal temperatures of the reaction systems. Results showed that the morphologies were closely related to the hydrothermal temperature. We obtained spherical, cubic, multi-armed and cross-like morphologies by adjusting the hydrothermal temperature. $Fe_{1.5}(PO_4)(OH)$ exhibited excellent electrochemical properties and good cyclic stability. The spherical morphology and small particle size improved the electrochemical performance of $Fe_{1.5}(PO_4)(OH)$ which may be due to the larger specific surface area of the small grain size, increasing the reaction interface to enhance the electrochemical activity of $Fe_{1.5}(PO_4)(OH)$ and shortening the diffusive distance of the lithium ions in cathode materials. Results investigated that the crystal morphology and particle size play important roles on the electrochemical properties of cathode materials. So the electrochemical properties of cathode materials of lithium ion batteries can be improved by controlling the morphology and particle size.

Acknowledgements

This work was carried out with financial support from the Project of Ability Development of Shanghai Science & Technology Commission (09230501400), the Research Foundation of the Ministry of Education (no: 2050255), China Aerospace Science & Technology Industry Group Corporation (DL-04) and the Natural Foundation of Shanghai (07ZR14042).

References

[1] Y. Wang, G. Cao, Advanced Materials 20 (2008) 2251–2269.
[2] A. Padhi, K. Nanjundaswamy, J.B. Goodenough, Journal of the Electrochemical Society 144 (1997) 1188–1194.
[3] J. Allen, T. Jow, J. Wolfenstine, Journal of Solid State Electrochemistry 12 (2008) 1031–1033.
[4] Y. Song, P.Y. Zavalij, M. Suzuki, M.S. Whittingham, Inorganic Chemistry 41 (2002) 5778–5786.
[5] C. Gerbaldi, G. Meligrana, S. Bodoardo, A. Tuel, N. Penazzi, Journal of Power Sources 174 (2007) 501–507.
[6] J. Ryu, C.B. Park, K. Kang, Chemical Communications 46 (2010) 7409–7411.
[7] Y.-S. Hong, K.S. Ryu, Y.J. Park, M.G. Kim, J.M. Lee, S.H. Chang, Journal of Materials Chemistry 12 (2002) 1870–1874.
[8] Z. Wang, S. Sun, F. Li, G. Chen, D. Xia, T. Zhao, W. Chu, Z. Wu, Materials Chemistry and Physics 123 (2010) 28–34.
[9] X. Yang, S. Zhang, J. Zhang, M. Xu, P. Ren, X. Li, L. Yan, Functional Materials Letters 4 (2011) 323–326.
[10] M. Lindberg, C. Christ, Acta Crystallographica 12 (1959) 695–697.
[11] G. Redhammer, G. Tippelt, G. Roth, W. Lottermoser, G. Amthauer, Physics and Chemistry of Minerals 27 (2000) 419–429.
[12] P.B. Moore, Science (New York, NY) 164 (1969) 1063.
[13] I. Fanfani, P. Zanazzi, Acta Crystallographica 22 (1967) 173–181.
[14] P.B. Moore, A.R. Kampf, Zeitschrift für Kristallographie 201 (1992) 263–281.
[15] Y. Song, P.Y. Zavalij, N.A. Chernova, M.S. Whittingham, Chemistry of Materials 17 (2005) 1139–1147.
[16] H. Yang, G. Costin, J. Keogh, R. Lu, R.T. Downs, Acta Crystallographica Section E: Structure Reports Online 63 (2007) i53–i55.
[17] M. Dollé, S. Patoux, T.J. Richardson, Journal of Power Sources 144 (2005) 208–213.
[18] J. Huang, L. Yang, K. Liu, Y. Tang, Journal of Power Sources 195 (2010) 5013–5018.